Title	Reduced surfactant uptake in three dimensional assemblies of VO(x) nanotubes improves reversible Li(+) intercalation and charge capacity
Authors	O'Dwyer, Colm;Lavayen, Vladimir;Tanner, David A.;Newcomb, Simon B.;Benavente, Eglantina;Gonzalez, Guillermo;Sotomayor Torres, Clivia M.
Publication date	2009
Original Citation	O'DWYER, C., LAVAYEN, V., TANNER, D. A., NEWCOMB, S. B., BENAVENTE, E., GONZÁLEZ, G. & TORRES, C. M. S. (2009). Reduced Surfactant Uptake in Three Dimensional Assemblies of VOx Nanotubes Improves Reversible Li+ Intercalation and Charge Capacity. Advanced Functional Materials, 19 (1), 1736-1745. doi: 10.1002/adfm.200801107
Type of publication	Article (peer-reviewed)
Link to publisher's version	http://onlinelibrary.wiley.com/doi/10.1002/adfm.200801107/pdf - 10.1002/adfm.200801107
Rights	© 2009 WILEY-VCH Verlag GmbH & Co. KGaA, Weinheim. This is the pre-peer reviewed version of the following article: O'DWYER, C., LAVAYEN, V., TANNER, D. A., NEWCOMB, S. B., BENAVENTE, E., GONZÁLEZ, G. & TORRES, C. M. S. 2009. Reduced Surfactant Uptake in Three Dimensional Assemblies of VOx Nanotubes Improves Reversible Li+ Intercalation and Charge Capacity. Advanced Functional Materials, 19, 1736-1745., which has been published in final form at http://dx.doi.org/10.1002/adfm.200801107
Download date	2024-04-19 23:19:42
Item downloaded from	https://hdl.handle.net/10468/975

University College Cork, Ireland
Coláiste na hOllscoile Corcaigh

Submitted to ADVANCED FUNCTIONAL MATERIALS

DOI: 10.1002/adfm.200801107

Reduced Surfactant Uptake in Three Dimensional Assemblies of VO_x Nanotubes Improves Reversible Li^+ Intercalation and Charge Capacity**

By Colm O'Dwyer, Vladimir Lavayen, David A. Tanner, Simon B. Newcomb, Eglantina Benavente, Guillermo González, Clivia M. Sotomayor Torres*

[*] Dr C. O'Dwyer
Department of Physics, and
Materials & Surface Science Institute,
University of Limerick, Limerick (Ireland)
Tel: +353.61.202288
E-mail: colm.odwyer@ul.ie

Dr V. Lavayen
Departamento de Física,
Universidad Técnica Federico Santa María,
Avenida España 1680,
2390123 Valparaíso (Chile)
and
Área de Ciências Naturais e Tecnológicas,
Centro Universitário Franciscano,
97010-032, Santa Maria – RS (Brazil)

Dr D. A. Tanner
Department of Manufacturing and Operations Engineering, and
Materials & Surface Science Institute,
University of Limerick, Limerick (Ireland)

Dr S. B. Newcomb
Glebe Scientific Limited
Newport, Co. Tipperary (Ireland)

Prof. E. Benavente
Department of Chemistry,
Universidad Tecnológica Metropolitana,
Av. Jose Pedro Alessandri,
Santiago (Chile)

Prof. G. González
Department of Chemistry,
Universidad de Chile, P. O. Box 653,
Santiago (Chile)

Submitted to ADVANCED FUNCTIONAL MATERIALS

Prof. Dr C. M. Sotomayor Torres
Institute for Research and Advanced Studies, ICREA,
08010 Barcelona, and Catalan Institute of Nanotechnology,
Edifici CM7, Campus Universitat Autonoma de Barcelona, 08193
Bellaterra (Spain)

[**] The support of the Science Foundation Ireland (SFI) under investigator award 02/IN.1/I172, the EU Network of Excellence P*h*OREMOST (FP6/2003/IST/2-511616), the University of Chile, and FONDECYT Grants 1050344, 1030102, 7050081, and 1050788 are gratefully acknowledged. V. L. acknowledges financial support from Rede Nacional de Pequisa em Nanotubos de Carbono, CNPq, Brazil, PBCT Grant ACT027, and FONDECYT Grant 1090683. Supporting Information is available online from Wiley InterScience or from the author.

Keywords: vanadium oxide, nanotubes, intercalation, batteries, energy storage

The relationship between the nanoscale structure of vanadium pentoxide nanotubes and their ability to accommodate Li^+ during intercalation/deintercalation is explored. The nanotubes are synthesized using two different precursors through a surfactant-assisted templating method, resulting in standalone VO_x (vanadium oxide) nanotubes and also nano-urchin. Under highly reducing conditions, where the interlaminar uptake of primary alkylamines is maximized, standalone nanotubes exhibit near-perfect scrolled layers and long-range structural order even at the molecular level. Under less reducing conditions, the degree of amine uptake is reduced due to a lower density of V^{4+} sites and less V_2O_5 is functionalized with adsorbed alkylammonium cations. This is typical of the nano-urchin structure. High-resolution TEM studies revealed the unique observation of nanometer-scale nanocrystals of pristine unreacted V_2O_5 throughout the length of the nanotubes in the nano-urchin. Electrochemical intercalation studies revealed that the very well ordered xerogel-based nanotubes exhibit similar specific capacities (235 mAh g^{-1}) to Na^+-exchange nanorolls of VO_x (200 mAh g^{-1}). By comparison, the theoretical maximum value is reported to be 240 mAh g^{-1}. The VOTPP-based nanotubes of the nano-urchin 3-D assemblies, however, exhibit useful

charge capacities exceeding 437 mAh g^{-1}, which is a considerable advance for VO_x based nanomaterials and one of the highest known capacities for Li^+ intercalated laminar vanadates.

1. Introduction

Low-dimensional nanomaterials such as nanotubes [1, 2], nanowires [3-5], nanobelts or nanoribbons [6-8], and other non-carbonaceous nanostructured compounds [9, 10] have attracted considerable attention in the past decade because of their novel and useful physical properties leading to numerous potential applications. Vanadium oxide-based low-dimensional products have been studied extensively [11-14]. Starting from the laminar V_2O_5 xerogel [15] numerous two dimensional organic-inorganic intercalation products have been obtained [16]. Most nanomaterials offer unusual (different from bulk) properties endowed by confined dimensions, and the overall behaviour can often exhibit a combination of bulk and surface properties [17].

Hydrothermal treatment (HT) of laminar composites, either those intercalated with long-chained organic molecules or those obtained directly from precursors, results in low-dimensional tubular products with practical quantitative yields [11, 16]. Many of these vanadate based nanostructures may be obtained in quantities of the order of grams [18, 19]. Together with the electrical and optical properties of vanadium oxide derivatives, this has encouraged its study as a potential new functional material. Varied applications such as optical switches [20, 21], field effect transistors [22] and as electrodes in Li^+ rechargeable batteries [23] have been reported and reviewed in detail.

In addition, the emerging energy resource crisis unambiguously highlights the need for new paradigms for energy storage; it is critical that consistently improved low-cost, lightweight, small volume and environmentally friendly energy storage/conversion devices are developed. To this end, the direct architecture of complex nanostructures is highly desirable, but controlled hierarchical structuring of choice materials still remains

challenging [24, 25]. Due to their size and shape dependent electronic and optical properties, significant effort has been made to control morphologies of transition-metal oxide nanostructures and to organize them into complicated three-dimensional structures using organic templates [26, 27]. The efficiency reached in the preparation of laminar and tubular nanostructures is necessary but not solely sufficient for integration of these materials in devices; specimens formed by ordered and dense arrays of uniform nanostructures are desired, hence the recent successful realization of the nano-urchin [15, 28]. Recent advances have clarified that Li^+ insertion into VO_x nanotubes and other nanostructured vanadium oxides has only recently been achieved [29, 30]; the next stage is the synthesis of more complex structures with greater volume for Li^+ insertion, but more importantly, exhibit identical or improved structural, chemico-mechanical and electrochemical properties as their individual counterparts.

Previous work [31] has conclusively shown that all vanadate structures are heavily reliant on the vanadate conformation and valency [19, 32, 33] after hydrothermal treatment and, as this work will outline, the resultant morphologies and constituent phases are dependent on the degree of hydration, or protonation, within the vanadium oxide lamina (and not solely on the intercalated structural organic template used) with a critical dependence on the precursors and hydrothermal conditions.

Thus, it is critical that for any potential further study and/or application of high density array analogues of individual low-dimensional structures, identical functionality with increased volumetric density must be achieved for direct ‘copy-paste’ application, which is paramount for metal-ion intercalation in rechargeable (secondary) battery technologies. Two independent groups have recently reviewed [34, 35] the potential advantages and associated potential 3-D structures for use as high intercalation volume for charge storage. The role of defect-rich vanadate nanostructures in improving the specific charge capacity upon Li^+

intercalation compared to those without defects [36] was outlined. Accurate characterization of the nanostructure, however, is essential in realizing new nanostructures than can accommodate interatomic layer cations and in classifying their applicability as open-access electrolyte scaffolds.

Here, we present the first definitive evidence of the influence of precursor hydration state during HT on the eventual composition and morphological characteristics of vanadium oxide nanotubes synthesized using two different precursors, and contrast the crystalline quality and intercalation volume variations between stand-alone nanotubes and those realised in nano-urchin that influence their specific charge capacity. The findings presented here evidence the local disorder and reduced surfactant uptake in vanadium oxide during hydrothermal treatment of nanotubes formed using the VOTPP precursor (see Experimental section). We observe and detail the formation of nanocrystals that result from localized regions of unreacted, monocrystalline orthorhombic V_2O_5 throughout the vanadate lamina in the nanotubes; no such findings are observed in nanotubes formed from the well-hydrated $V_2O_5 \cdot xH_2O$ xerogel. Differences in synthesis conditions chosen to achieve the same (morphology) product with different characteristics (greater density, higher intercalation volume etc.) can in certain cases affect the very material itself and its corresponding properties. For VO_x, this disorder vastly increases its specific charge capacity, charge/discharge cyclability and resistance to degradation.

2. Results and Discussion

Precursor influence on interlaminar spacing

Vanadium oxides are now very well understood from a phenomenological level and the myriad of reported applications have resulted in a greater understanding of their properties.

For a detailed overview of vanadium oxide, its lamellar phases, and properties that have been used in various applications, the reader is referred to a series of excellent and comprehensive reviews [17, 23, 31, 37, 38]. For the work reported here, the following characteristics are important: vanadium oxide nanotubes are synthesized from two different precursors, one containing a composite of HDA and VOTPP and the other containing HDA-intercalated xerogel. Both result in scrolled tubular morphologies after HT. We will demonstrate that the material precursor and synthetic conditions lead to a situation where the resulting nanotubes posses a different degree of interlaminar hydration/protonation correlated to, and influenced by, the nanoscale structural arrangement, the degree of surfactant binding uptake and resulting order in 3-D assemblies.

The orthorhombic crystal V_2O_5 (space group P*mnm*) is constructed by the stacking of 2D-like layers along its (010) direction and is composed by distorted edge-shared VO_5 pyramids, as depicted in **Fig. 1a** [37]. There are three known structurally non-equivalent types of oxygen centres in V_2O_5: single coordinated vanadyl oxygen O(1), double coordinated O(2) and bridging oxygen O(3) triply coordinated to vanadium atoms, all of which are important for spectroscopic analysis of the vibrational mode differences presented later. The structure of the (010) single-layer slab formed by VO_5 units sharing edges and corners and the positions of the non-equivalent O(1)–O(3) atoms [37] are also shown in **Fig. 1a**. The arrangement of the amine intercalated structure is a double bilayered product where the arrangement is periodically stacked back-to-back.

An important observation is that nanotubes formed from HT of the VOTPP precursor are found on high density radial arrays, or nano-urchin, whereas nanotubes from the xerogel tend to form as high yield, individual structures with no obvious preferred relative arrangement (of the tubes). Both sets of structures are shown in **Fig. 1b,c**. The inset to **Fig. 1b** shows a typical nanotube array section of a nano-urchin; the reduced overall order is apparent by contrast with

the nanotubes formed from the xerogel precursor in **Fig. 1c**. Even at high magnification, both sets of nanotubes look very similar and form from a similar scrolling mechanism. The TEM images in **Figs 1d,e** and **Fig. S1**, Supporting Information, highlight that both sets of nanotubes can have open ends, consist of a hollow core of ~20 nm diameter flanked by parallel rows of lattice fringes resulting from scrolled vanadate layers. These layers are separated by ~2.8 nm [8, 16] but as will be outlined later, the sub-nm differences in this interlaminar spacing can vary due the uptake/condensation of water molecules during synthesis [38] and associatd amine intercalation.

Selected area electron diffraction of the vanadate constituent of the nanotubes synthesized using both precursors (inset **Fig. 1c**) shows prominent polycrystalline diffraction rings (A, B, and C) with *d*-spacings matching the (200), (001), and (110), indicative of orthorhombic V_2O_5 with reconstructed lattice parameters of a_0 = 1.152 nm, b_0 = 0.356 nm, c_0 = 0.437 nm; Space Group = P*mnm*. The diffraction pattern of the highly turbostratic tube walls in **Fig. 1e** highlights the interlaminar spacing of 2.85 nm. Such nanotubes tend to be more ordered and structurally uniform even over their 5-15 μm length.

Figure 2a shows the X-ray diffraction analysis of the products from the reaction of VOTPP with HDA in a 2:1 molar ratio under normal conditions followed by a hydrolysis process, and also of the nanotubular product of the HT of the HDA intercalated xerogel. In **Fig. 2a**, the HT of the VOTPP-HDA reaction mixture leads to the formation of a pure mesophase formed by tubular species (*vide infra*) with an interlaminar distance of 2.87 nm. A set of less intense peaks appears at smaller *d* values (**Fig. 2a**, inset). These reflections are caused by the structure within the V_2O_5 layers and can be indexed to a square 2-D lattice with a = 0.611 nm. The {*hk*0} peaks do not display the typical asymmetric saw-tooth profile, suggesting that the registry mismatch or turbostratic disorder between the layers is markedly lower [8].

The absence of reflections of the type {*hkl*} with $l > 0$ is noteworthy. As the reflections of type {*hk*0} and {00*l*} are relatively sharp peaks, it is possible to define an approximate 3-D unit cell despite the bending of the layers, consistent with the presence of both non-intercalated, pure V_2O_5 and thin VO_x lamina due to reduced surfactant uptake. Such observations are typical of nanotubes formed from the VOTPP precursor, as recently verified by an independent study [28].

By comparison, the X-ray diffraction pattern for xerogel-based nanotubes shown in **Fig. 2b**, exhibits a slightly wider interlaminar distance (3.287 nm) and larger 2θ values do not exhibit any reflections consistent with a contribution from a 2- or 3-D V_2O_5 lattice structure (**Fig. 2b**, inset), indicating low-dimensionality and a highly turbostratic material. In fact, the only detectable {*hk*0} reflection is that of (110), arising from the stacking of the vanadium oxide molecular layers to form the lamina. The reduction in 2-D crystallinity of the vanadium oxide lamina, confirms the highly turbostratic arrangement of the double bilayers comprising the nanotubes' multiwalled architecture. This point if further emphasized by noting that both diffraction patterns in **Figs 2a,b** exhibit (001) diffraction contributions with a laminar tendency from a second phase identified as the quasi-crystalline bilayered amines (indicated by **). The degree of interlaminar bilayered ordering is markedly lower in VOTPP tubes in the nano-urchin, as it directly affects the degree of vanadium ion reduction, whereas intense peaks are observed for xerogel-based nanotubes; both (001) and (002) reflections are measured. The difference in overall structural uniformity is apparent from the TEM images of individual nanotubes from each system (see **Fig. S1**, Supporting Information).

To quantitatively analyze the difference in interlaminar distance, measurements of both the vanadium oxide lamina thickness and the interlaminar spacing were acquired for both types of nanotubes by HRTEM. The images in **Fig. 3** allow quantitative measurement of actual interlaminar distances in both types of nanotubes by quantifying the normalized grey-

scale intensities from calibrated images [39], weighted by their respective scattering factors. **Figures 3a,b** shows representative HRTEM images of typical tubular morphologies from VOTPP and xerogel-based synthetic routes, respectively; the degree of uniformity as observed in **Figs 1** and **S1**, is markedly different, where VOTPP-based nanotubes exhibit variations in tube wall thickness, internal diameter and evidence for a less ordered scrolling of the vanadate layers observable through diffraction contrast.

Averaged measurements of the overall interlaminar spacings from both systems, shown in **Figs 3c,d**, yields values of 2.855 nm and 3.340 nm for the VOTPP- and xerogel-based VO_x nanotubes, respectively, in good agreement with XRD measurements. The electron diffraction measurement in **Figs 3e** corroborates the observations from two standpoints. Firstly, SAED patterns from xerogel-based nanotubes show two sets of two pronounced diffraction spots, where set (A) in **Fig. 3e** corresponds to a 2.85 nm distance and the outer set (B) corresponds to the distance caused by the intercalated amine bilayers [40]. This biphasic diffraction contribution was previously observed in the XRD diffraction data in **Fig. 2** and implies the presence of a quasi-crystalline amine bilayer sandwiched between highly crystalline and turbostratic V_2O_5 lamina.

Variation in surfactant uptake in nanotubes and nano-urchin

It is apparent that the hydration state and surfactant packing density of the precursors have measurable effects on the overall structure and morphological properties of the nanotubes [41, 42], as evidenced by XRD and TEM data. Since the choice of precursor can determine the long-range structural order and the potential for 3-D assembly formation during HT, we used HRTEM to determine the effect of hydration state and amine uptake/adsorption during HT to determine why a 3-D array of nanotubes formed using the VOTPP precursor (resulting in nano-urchin) would have less ordered nanotubes.

HRTEM analysis of the nanotubes formed using VOTPP was conducted at various stages of growth; representative images are shown in **Fig. 4**. The bright-field image in **Fig. 4a** shows individual nanotubes from a nano-urchin during their scrolling stage; the leading edge of a single lamina is outlined in **Fig. 4b**. The highly defective lamina observed in **Fig. 4b** are consistent with the lower degree of uniformity with VOTPP-based nanotubes where we routinely observed lattice plane termination dislocations, laminar curvature, buckling and a non-uniform hollow core (see **Fig. S2**, Supporting Information). Dark-field imaging, however, reveals the presence of a crystalline phase throughout the length of the tubes. The two dark-field images in **Figs 4c,d** show that these nanocrystals (formed by bound VO_5 units that do not have adsorbed alkylammonium ions) are distributed throughout the nanotube. It is worth noting that no nanocrystals are found on the organic (amine) sheath/layer, by comparing **Figs 4 a–d** and **Fig. S2**.

Further HRTEM studies were carried out to determine the crystalline phase of the nanocrystalline regions and to investigate any preferential or site-selective placement (or dispersion) throughout the nanotubes. These observations, it must be stated, do not occur during electron beam irradiation and the intensity of diffraction spots did not change during prolonged imaging. **Figure 5** shows corresponding bright and dark field TEM images of a portion of the nanotube walls of a VOTPP-based nanotube. It can be observed that regions of the VO_x lamina contain small crystals in **Fig. 5b** that are typically located at regions of higher scattering (from V atoms) in **Fig. 5a**, similar to **Fig. 4**. Higher magnification images and associated SAED in **Fig. 5** confirm the presence of orthorhombic V_2O_5 with reasonable monodispersivity throughout the lamina. **Fig. S3**, Supporting Information, shows another portion of a nanotube wall where the dispersion is more evident. Analysis of the nanocrystalline regions in **Fig. 5c**, which was taken from several areas of many tubes, shows that the average size of the nanocrystals is 0.2–0.5 nm.

As was seen in **Figs 4a** (at D and E) and **5b**, certain regions of the nano-urchin nanotube walls contain relatively very large areas of unreacted V_2O_5 (much greater than 0.5 nm). **Figure 6** shows corresponding pairs of bright and dark field TEM images of such regions. **Figs 6a,b** show two nanotubes at early stages of formation. The stacked and scrolled layers are such that the outer layer is on top (in projection). The dark field image shows the large regions where the degree of amine intercalation is locally reduced, exposing unreacted V_2O_5. **Figs 6c,d** show the crystalline regions at the tips of 'younger' nanotubes, similar to those shown in **Fig. 4a**. Here, SAED conclusively shows that the brilliant regions of the nanotubes are monocrystalline orthorhombic V_2O_5. Thus, for VOTPP-based nanotubes, the reduced hydration state results in a less than perfect uptake of amines as alkylammonium ions resulting in local disorder and regions of unreacted vanadate.

Since the respective interlaminar spacings of the two material systems are different, the observations can be ascribed to different quantities of surfactant molecules incorporated between the layers due, primarily, to the cationic exchange-controlled variation in vanadium valency in tandem with corresponding variations in vanadate hydration. Thus, there are more amine molecules incorporated in better ordered xerogel-based nanotubes, facilitated by electrostatic binding caused by their reduction to alkylammonium ions in the presence of sufficient water. Furthermore, in contrast to previous reports [36], we did not employ any reducing agent during synthesis to distinctly vary or control the vanadium valency ratio (V^{4+}:V^{5+}).

Infrared vibrational characterisation of surfactant uptake

For comparison of the inorganic-organic nanostructured lamellar precursors and their resulting nanotubular products at the molecular-interaction level, FTIR spectra were acquired from both types of nanotubes. The spectral information is divided in two parts: the

contribution from the intercalated surfactant and their interaction with the VO_x, and the vibrational characteristics of the VO_x itself. Both nano-urchin (VOTPP-based) and stand-alone nanotubes (xerogel-based) exhibit characteristic bands between 3000 and 3300 cm^{-1} attributed to the N–H vibrational modes, shown in **Figs 7a** and **7b**, respectively. The principle difference here is the detection of particular N-H vibrations from alkylammonium cations in xerogel-based nanotubes at 3050 and 3130 cm^{-1} as shown in **Fig. 7a**, whereas we observe a uniform band of vibrations from the $–NH_2$ headgroup of the amines in the nano-urchin (**Fig. 7b**). These differences result from reduction in the amount of successfully intercalated amines in the presence of water in VOTPP-based nanotubes. Comparison to pure orthorhombic V_2O_5 and the VO_x-amine lamellar precursor prior to HT, shown in **Fig. 7c**, shows the presence of OH groups (between 3300 and 3700 cm^{-1}) and a broad band of N-H vibrations. The axial stretching modes of the aliphatic C-H groups at 2917 and 2852 cm^{-1} are consistent in both types of nanotubes. The influence of the degree of alkylammonium adsorption is also seen at lower wavenumbers. For nano-urchin tubes, the H-N-H wagging vibrations are almost non-existent (**Fig. 7a**) whereas for stand-alone nanotubes shown between 1500-1650 cm^{-1} the discrete vibrations are again specifically linked to alkylammonium ions adsorbed on V_2O_5. The C-N stretching vibration is also observed for nano-urchin VOTPP-based tubes consistent with a lesser degree of adsorption and greater degrees of freedom. The same modes are not observed for the higher quality xerogel-based tubes.

Turning to the higher frequency heavy atom-light atom region, the V-O vibrational modes give further evidence for the hydration state (protonation) influence on the degree of surfactant uptake or binding. Both xerogel and VOTPP-based nanotubes (**Figs 7a,b**) exhibit modes from the important vanadyl oxygen (V=O) stretching and the edge-shared oxygen bending vibrations of the V-O-V species. The nano-urchin tubes (**Fig. 7a**) show V=O bands at 949 and 999 cm^{-1} corresponding to orthorhombic γ-V_2O_5 in its V^{5+} state. The stand-alone

nanotubes also evidence these vibrations but at higher frequencies indicative of α-V_2O_5 in its V^{4+} state with a correspondingly lower intensity due to the presence of hydroxyl groups formed by the reduction of alkylamine to alkylammonium. The reduced intensity indicates that only certain regions of the xerogel-based nanotubes' lamella contain V=O bonds in the same conformation as the nano-urchin tubes, and that in regions where V-O^- terminal groups are formed, interlaminar alkylammonium cation uptake is possible. Analysis of the V-O-V bond vibrations corroborates this suggestion; we observe a distinct V-O-V conformation in the better quality xerogel-based nanotubes where at 640 cm^{-1} in **Fig. 7b**, the V-O-V vibration characteristic of six-coordinated vanadium is observed rather than the band of modes observed for the VO_5 units (750–840 cm^{-1}) observed in the VOTPP-based tubes. This particular vibration is directly related to the ordered orthorhombic structure characteristic of pure V_2O_5, shifted to higher frequencies (lower wavenumbers) due to the electrostatic uptake of the alkylammonium cation. This is most apparent when compared to the same wavenumber region for pure V_2O_5 shown in **Fig. 7d**. Here, the V=O and V-O-V bonds are very distinct, and more closely related to the xerogel-based tubes in terms of vanadate ordering and structure. The V_2O_5 and amine mixture prior to HT, also shown in **Fig. 7d**, clearly exhibits several modes for these bonds consistent with the influence of the amine molecules and the OH group presence shown in **Fig. 7c**.

Thus, the structural rigidity and order that defines the nanotube walls is apparent by noting that only pre-HT compounds or pure V_2O_5 display asymmetrical O-$(V)_3$ deformation vibrations of the vanadyl polyhedra. Thus, the overall picture is that the level of laminar hydration allows for improved surfactant binding and better structural order in the vanadium oxide as evidenced by the specific differences in the vibrational modes and energies of N-H, N-H-N, V=O, V-O-V and C-N bonds between both types of nanotubes.

Recent measurements have verified the relationship between the vanadium valency ratios and the degree of curvature in scrolled VO_x nanotubes [19, 28]. The associated reduction in the ratio of V^{5+} to V^{4+} allows the nanostructures to form with less laminar distortion during HT by increasing the inorganic charge density (more V-O^- groups formed by reaction of OH^- groups with V=O bonds) and more effective binding uptake of the surfactant. At a more fundamental level, the findings are corroborated by previous in-depth periodic DFT studies [43], which have conclusively shown that the amine headgroup adsorbs preferentially at Brønsted acid sites of the V_2O_5 (010) surface and furthermore, it is also confirmed that the adsorption ability decreases in the order corresponding to the hydroxyl groups: $O_1H > O_3H > O_2H$. This order was shown to indicate that the adsorption of alkylammonium in the presence of O_1H groups is seemingly the most favourable [44].

The reaction path is dictated by a significantly reduced number of V=O bonds in xerogel-based nanotubes and not in those from VOTPP-based precursors, in tandem with the opposite trend for alkylammonium cations (which only display select vibrations in xerogel-based nanotubes due to their improved adsorption). The amines are hydrolyzed by water to form alkylammonium ions and hydroxide ions. The Lewis base hydroxides interact with the open space of the square pyramidal coordination of the VO_5 unit cell, where the π-electrons of the V=O are taken up by the oxygen as a lone-pair, which can attract alkylammonium cations through electrostatic forces, as depicted in **Scheme 1**. Interlaminar uptake of the amines (in their charged alkylammonium state) must be accounted for in the VO_x layers where V_2O_5 units now become six-coordinated. This reaction process explains the observation of unreacted pure V_2O_5 when it does not go to completion due to the V^{5+} and V^{4+} having different conformations [19] and different associated binding uptake properties. We observe specific N-H vibrations consistent with NH_2 groups by FTIR in the nano-urchin tubes, shown in **Fig. 7a**, consistent with the presence of unreacted amines.

Electrochemical intercalation, charge capacity and cycling performance

The electrochemical charge storage and cycling performance of both types of nanotube-containing systems were also investigated. In **Fig. 8** we present the cyclic voltammetric response of the xerogel-based and VOTPP-based nanotubes (nano-urchin). **Figure 8a** shows the first and fiftieth cycles of the xerogel-based nanotubes between 1.5 and 4.0 V (vs. Li^+/Li). The first cycle exhibits the well-documented oxidation and reduction peaks associated with phase changes occurring in the vanadium oxide lattice upon intercalation of Li^+ [45]. The total capacity decreases with increasing cycle number for the xerogel-based system in a similar manner to what is normally observed, exhibiting a concomitant irreversible positive shift in the cathodic peak from 2.6 to 2.72 V over 50 cycles indicating a permanent structural change. Of significant interest is the considerably higher specific charge capacity of the nano-urchin tubular material even after 50 cycles, shown in **Fig. 8b**. Furthermore, the height of the current peak in the cyclic voltammetric response decreased negligibly (by comparison with the variation observed for xerogel-based nanotubes) over these 50 cycles. The voltammetric curve from the nano-urchin in **Fig. 8b**, shows a cathodic peak at a more positive potential (to that of the xerogel-based nanotubes) of 2.8V which showed negligible shifting over 50 cycles.

The discharge response shown in **Fig. 8c** for the nano-urchin is noted to be similar to pure orthorhombic V_2O_5, displaying multiple redox couples which themselves indicate structural transformations from the α-phase, through the ε, δ, and γ- phases and finally the reversible ω-$Li_xV_2O_5$ phase [46]. By comparison, the xerogel-based nanotubes exhibit similar α, ε, and δ-$Li_xV_2O_5$ phase transformations, but at lower potentials; the γ- and ω-phases occur at similar potentials for both materials. The specific charge capacity of the first cycle, also shown in **Fig. 8c**, show conclusively that the nano-urchin can hold a considerably higher specific

charge capacity (437 mAh g^{-1}) than the nanotubes (235 mAh g^{-1}) which have a higher degree of crystalline uniformity.

The differences in specific capacity are most probably related to the quantity of organic interlaminar surfactant. We know that the nanotubes of the nano-urchin possess a considerable volume of unreacted and pure V_2O_5 throughout its mostly scrolled laminar morphology, resulting in less residual surfactant between the VO_x layers compared to xerogel-based nanotubes. This is a direct result of a lower degree of surfactant uptake/electrostatic binding and consequently provides a more open pathway for Li^+ interlaminar intercalation/diffusion [47] giving higher capacities. The structural disorder is more likely to accommodate the volumetric changes associated with the reduction of V^{5+} to V^{4+} during intercalation, since these ions exhibit remarkable different sizes [48]: 0.495 Å radius of V^{5+} ions versus much larger 0.86 Å radius V^{4+} ions. This deleterious volumetric effect in silicon-based battery anodes has only recently been overcome by utilizing nanostructured arrays of Si nanowires [49].

3. Conclusions

In summary, the formation of VO_x nanotubes using an alkyl amine structure-directing template by wet chemistry is a complicated process which includes van der Waal's interaction between alkyl chains, electrostatic interaction between the organic and inorganic components together with transition metal oxide polymerization resulting in the final nanostructure. However, both molecular and nanometer-level local structure has a considerable effect on the specific charge capacity. What is now clear is that the initial synthesis precursors can affect the local structure and intercalation volume and properties, even in the absence of specific environmental or synthetic conditions, or even reducing agents. The turbostratic lamellar structure undergoes laminar scrolling during hydrothermal treatment; with a greater surfactant

uptake between lamina, the stronger the hydrophobic interactions and thus an increased level or order is observed throughout the layers comprising the nanotube. Conversely, the valency of the vanadium ions as a result of the precursor chemistry, can result in non-interacting vanadia and the observation of the nanoscale (~0.5 nm) regions of remnant or unreacted V_2O_5 along the walls of more disordered nanotubes. Such disordered nanotubes (on the nanoscale at molecular level) produce higher specific capacities and better cyclability due to their ability to allow considerable phase changes without the typically observed restrictions to high volume intercalation caused by limited interlaminar space in more ordered structures [49]. We now know that the increased accessibility of V_2O_5 sites for metal ions further enhanced by a higher density of redox sites compared to pristine nanotubes that contain a high intercalated volume fraction of alkylammonium ions in the interlaminar spacings.

The very well ordered xerogel-based nanotubes exhibit similar specific capacities (235 mAh g^{-1}) to Na^+-exchange nanorolls of VO_x (200 mAh g^{-1}) [29]. By comparison, the theoretical maximum value is reported [50] to be 240 mAh g^{-1}. The VOTPP-based nanotubes of the nano-urchin, however, exhibit remarkable charge capacities exceeding 437 mAh g^{-1}, which is a considerable advance for VO_x based nanomaterials and one of the highest known capacities for Li^+ intercalated laminar vanadates.

The improved electrochemical properties observed in novel vanadium oxide nano-urchin are attributed to the increased volumetric density for ion intercalation, and shorter diffusion paths to the intercalation/redox sites. This is caused by a reduced intercalated alkylammonium volume fraction influenced by the hydration state of the V_2O_5 during synthesis. In addition, these structures permit the greatest freedom for dimensional change that accompanies intercalation and extraction reactions.

4. Experimental

Synthesis of the Vanadium Oxide Nano-Urchin: A solution of 10^{-3} mol of 1-hexadecylamine (HDA), $C_{16}H_{33}NH_2$ (Aldrich, 99%), in pure ethanol (10 mL), previously degassed by repetitive freeze-thaw cycling in an argon vacuum, was mixed with vanadium tri-isopropoxide (VOTPP, 2×10^{-3} mol), $[(CH_3)_2CHO]_3VO$ (Aldrich). The yellow solution, obtained after vigorous stirring in an argon atmosphere for 1 h, was then hydrolyzed by adding deionized water (15 mL). An orange suspension was obtained after continuous stirring for 24 h. The hydrothermal treatment (HT) of the orange suspension was performed in a Teflon lined autoclave at 180^{o}C for 7 days. From the resulting dark suspension, a dark solid was separated, washed with pure ethanol and water, dried under vacuum (1.33×10^{-3} mbar) for 48 h, and stored in an argon atmosphere.

Synthesis of the Vanadium Oxide Nanotubes: A mixture of *t*-butyl alcohol and orthorhombic V_2O_5 (Aldrich, 99%) was refluxed for 6 h to form the xerogel. Water was added to the resulting dark yellow solid and the remaining *t*-butyl alcohol was removed with excess water in vacuum. Water was then added to yield a suspension. The material was aged at room temperature yielding a red-brown colloidal V_2O_5. The xerogel and a primary amine, 1-hexadecylamine (HDA), mixed in a molar ratio of 1:2, were stirred in ethanol for 2 h and left to age for 2 days. The composite was transferred into a Teflon-lined autoclave and held at 180^{o}C for 3 days under auto-generated pressure in a sand bath. The product was washed with deionized water and alcohol several times and dried under vacuum.

Methods of Characterization: X-ray powder diffraction characterization was performed using a Siemens D5000 diffractometer (Cu Kα, λ = 0.15418 nm, operation voltage 40 kV, current 30 mA). The morphological characterization of the nanostructured products was performed by field-emission scanning electron microscopy (FESEM) using a HITACHI S-4800 FESEM

operating at beam voltages between 1 and 10 kV. Electron transparent specimens were prepared by ion-milling techniques or solution deposition and placed on a holey carbon support. Transmission electron microscopy (TEM) and selected area electron diffraction (SAED) were conducted using a JEOL JEM 2011 and 2000FX TEM operating at 200 kV. The chemical composition of the samples was determined by elemental chemical analysis using a SISONS model EA-1108 analyzer. The Fourier transform infrared (FTIR) spectra were recorded using a KBr pellet technique on a Perkin-Elmer Series 2000 apparatus in the region 4000-450 cm^{-1}.

For intercalation/deintercalation experiments, the electrochemical cell comprised a working cathode prepared using a stainless steel mesh dipped in an ethanolic solution of either VO_x nanotubes or nano-urchin, carbon black and poly(tetraflouroethylene) (PTFE) in a mass ratio of 75:15:10. Lithium pellets and foil served as counter and reference electrodes, respectively. Cyclic voltammetry and galvanostatic charge/discharge experiments were performed in a 1 mol dm^{-3} $LiClO_4$:ethylene carbonate (1:1 v/v) electrolyte. The cyclic voltammograms were acquired at a scan rate of 1 mV s^{-1} between 1.5 and 4.0 V vs. Li^+/Li using a CH Instruments Model 660C electrochemical workstation.

Received: ((will be filled in by the editorial staff))
Revised: ((will be filled in by the editorial staff))
Published online: ((will be filled in by the editorial staff))

[1] S. Iijima, *Nature* **1991**, *354*, 56.

[2] P. M. Ajayan, S. Iijima, *Nature* **1992**, *358*, 23.

[3] A. M. Morales, C. M. Lieber, *Science* **1998**, *279*, 208.

[4] Z. W. Pan, Z. R. Dai, Z. L. Wang, *Science* **2001**, *291*, 1947.

[5] Y. H. Gao, Y. Bando, T. Sato, *Appl. Phys. Lett.* **2001**, *79*, 4565.

[6] W. S. Shi, H. Y. Peng, N. Wang, C. P. Li, L. Xu, C. S. Lee, R. Kalish, S. T. Lee, *J. Am. Chem. Soc.* **2001**, *123*, 11095.

[7] P. Gomez-Romero, *Adv. Mater.* **2001**, *13*, 163.

[8] F. Krumeich, H.-J. Muhr, M. Niederberger, F. Bieri, B. Schnyder, R. Nesper, *J. Am. Chem. Soc.* **1999**, *121*, 8324.

[9] R. Tenne, L. Margulis, M. Genut, G. Hodes, *Nature* **1992**, *360*, 444.

[10] Y. Feldman, E. Wasserman, D. J. Srolovich, R. Tenne, *Science* **1995**, *267*, 222.

[11] M. E. Spahr, P. Bitterli, R. Nesper, M. Muller, F. Krumeich, H.-U. Nissen, *Angew. Chem. Int. Ed.* **1998**, *37*, 1263.

[12] H.-J. Muhr, F. Krumeich, U. P. Schonholzer, F. Bieri, M. Niederberger, L. J. Gauckler, R. Nesper, *Adv. Mater.* **2000**, *12*, 231.

[13] M. Niederberger, H.-J. Muhr, F. Krumeich, F. Bieri, D. Gunther, R. Nesper, *Chem. Mater.* **2000**, *12*, 1995.

[14] G. R. Patzke, F. Krumeich, R. Nesper, *Angew. Chem. Int. Ed.* **2002**, *41*, 2446.

[15] C. O'Dwyer, D. Navas, V. Lavayen, E. Benavente, M. A. Santa Ana, G. Gonzalez, S. B. Newcomb, C. M. Sotomayor Torres, *Chem. Mater.* **2006**, *18*, 3016.

[16] C. O'Dwyer, V. Lavayen, S. B. Newcomb, E. Benavente, M. A. Santa Ana, G. Gonzalez, C. M. Sotomayor Torres, *Electrochem. Solid-State Lett.* **2007**, *10*, A111.

[17] G. Z. Cao, *Nanostructures and Nanomaterials, Synthesis, Properties and Applications*, Imperial College Press, London **2004**.

[18] V. Lavayen, C. O'Dwyer, M. A. Santa Ana, S. B. Newcomb, E. Benavente, G. Gonzalez, C. M. Sotomayor Torres, *Phys. Status Solidi B* **2006**, *243*, 3285.

[19] C. O'Dwyer, V. Lavayen, S. B. Newcomb, M. A. Santa Ana, E. Benavente, G. Gonzalez, C. M. Sotomayor Torres, *J. Electrochem. Soc.* **2007**, *154*, K29.

[20] J. F. Xu, R. Czerw, S. Webster, D. L. Caroll, J. Ballato, R. Nesper, *Appl. Phys. Lett.* **2002**, *79*, 1711.

[21] M. Ando, K. Kadono, M. Haruta, T. Sakaguchi, M. Miya, *Nature* **1995**, *374*, 625.

[22] G. T. Kim, J. Muster, V. Krstic, J. G. Park, Y. W. Park, S. Roth, M. Burghard, *Appl. Phys. Lett.* **2000**, *76*, 1875.

[23] Y. Wang, G. Z. Cao, *Chem. Mater.* **2006**, *18*, 2787.

[24] Y. Huang, X. Duan, Q. Wei, C. M. Lieber, *Science* **2001**, *291*, 630.

[25] A. P. Alivisatos, *Science* **1996**, *271*, 933.

[26] Y. Sun, Y. Xia, *Science* **2002**, *298*, 2176.

[27] D. Yu, W. V. Yam, *J. Am. Chem. Soc.* **2004**, *126*, 1320.

[28] M. Roppolo, C. B. Jacobs, S. Upreti, N. A. Chernova, M. S. Whittingham, *J. Mater. Sci.* **2008**, *43*, 4742.

[29] S. Nordlinder, K. Edström, T. Gustafsson, *Electrochem. Solid-State Lett.* **2001**, *4*, A129.

[30] S. Nordlinder, L. Nyholm, T. Gustafsson, K. Edström, *Chem. Mater.* **2006**, *18*, 495.

[31] M. S. Whittingham, *Chem. Rev.* **2004**, *104*, 4271.

[32] J. Cao, J. Choi, J. L. Musfeldt, S. Lutta, M. S. Whittingham, *Chem. Mater.* **2004**, *16*, 731.

[33] V. Petkov, P. Y. Zavalij, S. Lutta, M. S. Whittingham, V. Paranov, S. Shastri, *Phys. Rev. B* **2004**, *69*, 085410.

[34] B. Dunn, *Chem. Rev.* **2003**, *104*, 4463.

[35] P. G. Bruce, B. Scrosati, J.-M. Tarascon, *Angew. Chem. Int. Ed.* **2008**, *47*, 2930 and references therein.

[36] D. Sun, C. K. Kwon, G. Baure, E. Richman, J. MacLean, B. Dunn, S. H. Tolbert, *Adv. Funct. Mater.* **2004**, *14*, 1197.

[37] P. Y. Zavalij, M. S. Whittingham, *Acta Cryst.* **1999**, *B55*, 67.

[38] J. Livage, *Chem. Mater.* **1991**, *3*, 578.

[39] ImageJ, National Institutes of Health, USA.

[40] S. Cheng, H.-D. Hwang, G. E. Maciel, *J. Mol. Struct.* **1998**, *470*, 135.

[41] Y. Wang, H. Shang, T. Chou, G. Z. Cao, *J. Phys. Chem. B* **2005**, *109*, 11361.

[42] V. Petkov, P. N. Trikalitis, E. S. Bozin, S. J. L. Billinge, T. Vogt, M. G. Kanatzidis, *J. Am. Chem. Soc.* **2002**, *124*, 10157.

[43] X. Yin, H. Han, I. Gunji, A. Endou, S. Salai Cheettu Ammal, M. Kubo, A. Miyamoto, *J. Phys. Chem. B* **1999**, *103*, 4701.

[44] N.-Y. Topsøe, *Science* **1994**, *265*, 1217.

[45] C. Delmas, H. Cognac-Auradou, J. M. Cocciantelli, M. Ménétrier, J. P. Doumerc, *Solid State Ionics* **1994**, *69*, 257.

[46] M. Winter, J. O. Besenhard, M. E. Spahr, P. Novak, *Adv. Mater.* **1998**, *10*, 725.

[47] C. O'Dwyer, V. Lavayen, M. A. Santa Ana, E. Benavente, G. Gonzalez, C. M. Sotomayor Torres, *Res. Lett. Phys. Chem.* **2007**, 32528.

[48] G. Gu, M. Schmid, P.-W. Chiu, A. Minett, J. Fraysse, G.-T. Kim, S. Roth, M. Kozlov, E. Munoz, R. H. Baughman, *Nat. Mater.* **2003**, *2*, 316.

[49] C. K. Chan, H. Y. Peng, G. Liu, K. McIlwrath, X. F. Zhang, R. A. Huggins, Y. Cui, *Nat. Nanotech.* **2008**, *3*, 31.

[50] S. Nordlinder, J. Lindgren, T. Gustafsson, K. Edström, *J. Electrochem. Soc.* **2003**, *150*, E280.

TOC Entry

Vanadium oxide nano-urchin and nanotubes are observed to have varying degrees of crystalline order and uniformity depending on the precursor used and its hydration state during synthesis, resulting in reduced interlaminar alkylammonium cation uptake and exposure of nanocrystalline regions of pure orthorhombic V_2O_5 throughout the length of nanotubes (See Figure). Less ordered nanotubes result in improved specific charge capacities and cyclability.

Battery Nanotubes

Colm O'Dwyer, Vladimir Lavayen, David A. Tanner, Simon B. Newcomb, Guillermo González, Eglantina Benavente, Clivia M. Sotomayor Torres ■<B>…<B>■

Reduced Surfactant Uptake in Three Dimensional Assemblies of VO_x Nanotubes Improves Reversible Li^+ Intercalation and Charge Capacity

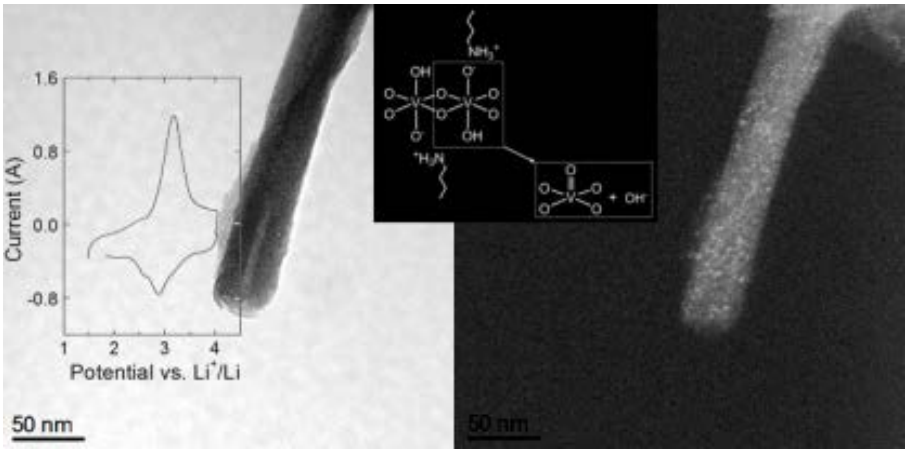

C. O'Dwyer et al./Reduced Surfactant Uptake and Improved Charge Capacity in VO_x Nanotubes